Detection of Image Splicing using Illuminant Color Estimation

Yu Fan, David Helbert, Anne-Sophie Capelle-Laizé, Philippe Carré, Christine Fernandez-Maloigne

Detection of Image Splicing using Illuminant Color Estimation

Yu Fan, David Helbert, Anne-Sophie Capelle-Laizé ,Philippe Carré, and Christine Fernandez-Maloigne

September 23, 2019

Abstract

Digital image forensics is a set of techniques used for digital image forgery detection and is widely used to certify the content or the authenticity of a document. The splicing operation, which crops and pastes one or several regions from separate images, is a common technique used for image forgery. In the literature, most image forgery detection techniques are based on machine learning. Only a few methods take advantage of physical features to detect the tampering. In this paper, we propose a new method to detect image splicing from an analysis of regions of interest in the uv chromaticity space. Their pixels are compared to the Planckian locus and the closest ones, seen as achromatic, are stored in a weighted histogram depicting Gaussian distribution. After a selection of the suitable Gaussians, the illuminant color is estimated. Results on spiced images are presented and discussed.

Keywords: Color image forensics, physical features

1 Introduction

More than 350 million photos have been uploaded every day on Facebook on average, throughout 2013[1]. On that same year, due to the popularity of smartphones, more than 660 billion of photos have been taken, which increased to 1.1 trillion in 2016 [2]. There is no doubt that our everyday lives are replete with images coming from numerous media, let it be television, newspaper, news site or social network. Given the rising threat of "fake news", it would be interesting to know the ratio of manipulated images, which is not at all a straightforward matter. According to a 2015 poll, while 76% of press photographers regard image manipulation as a "serious problem", 25% admit that they sometimes alter the content of images, other than by cropping [3]. This being only related to the press, we would also have to include all the pictures fraudulently submitted in the information flow and shared all across social medias, which is impossible to estimate. Indeed, digital image forgery is nowadays accessible to the general public through the use of numerous powerful and low-cost image editing software. From this assessment, we can admit that being able to trust the authenticity of any given digital image has become quite difficult [4, 5] while having the means to detect image forgery is now primordial: this is the purview of digital image forensics, a set of techniques used for image forgery detection [6, 7], that is to say certifying the content or the authenticity of documents and their data[8]. Even though the authenticity of an image can be proved by directly embedding a digital watermark into it [9], not all hardware can insert such a watermark before the manipulation of the image. To overcome this difficulty, blind image forensics has been proposed to deal with the image tampering without inserting any security information. It assumes that even if the image forgeries may not leave usual traces that would indicate tampering, they also alter the underlying patterns that are introduced by imaging devices of an original untampered image. A digital image can be tampered in many ways, such as by geometric transformations, color adjustments, copy-moves and so on. One of the most common image manipulation method consists in cropping and pasting one or several regions from the separate images, a technique known as splicing. In this article, we will focus on the detection of images that have been spliced.

Over the past few years, many techniques and methodologies have been proposed to deal with image forgeries linked to image splicing [6, 10, 11]. Previous works can generally be classified into three categories. The first category identifies the manipulated images by detecting the statistical anomalies, for example in the frequency domain [12, 13, 14]. Deep learning based forensic methods are proposed to design image splicing and detect image manipulations [15, 16]. Many methods in this category are based on algorithms needing preconditions, such as the ones based on a learning strategy, requiring a the construction of a model to generate results. In addition, some of them are weak against anti-forensics techniques that remove the detectable traces found in the images and used by these methods. The second category evaluates the changes in the features introduced by digital data acquisition devices such as cameras, scanners, etc. Most of the methods in this category require information about the source acquisition device in order to compare the inherent patterns extracted from the sample images. Some examples of the inherent patterns are the sensor pattern noise [17], aberrations produced by a lens [18] and so on. The physically based techniques of the last category detect the inconsistency of the scene properties. Among those, the illumination condition has been considered as an indicator for forgery detection. The illuminant-based methods are either geometry-based or color-based. The geometry-based methods detect the inconsistencies of the direction of light source between the sample regions on the scene [19, 20, 21, 22], while the color-based ones detect the illuminant color inconsistencies [23, 24, 25, 26].

In this paper, we will focus on a color-based method for splicing operation detection. In recent years, a lot of methods have been proposed for illuminant estimation [27, 28]. However, very few of them are applied to the security field. In addition, most of the methods for illu-

(a) The first dataset, with pictures both taken indoors and outdoors.

(b) Subset of the images used in the sliced pictures.

Figure 1: Preview of pictures.

minant estimation are based on the Lambertian model [29] and some of them estimate the illuminant using the dichromatic reflection model [30, 31]. We propose to adapt a method of illuminant estimation for splicing operation detection based on Mazin and Delon [32], using the Lambertian model.

The contributions of this work are as it follows: we also improved the way the illuminant colors are estimated by making it more quick and reliable. Secondly, we added a practical way to analyze the illuminant estimation to detect potential tampering.

A collection of images was created by using a *Nikon D300S* camera with two 60mm and 90mm lenses, is composed of 25 high-resolution pictures and is showcased in Section 4. Each set features indoors and outdoors photographs of various scenes depicting sets of objects, humans or simple background sceneries, with a majority of scenes containing specular highlights. Since our method relies on operations made directly on the pixels values of the image, the pictures have been taken in RAW format with a 14-bit depth to preserve their quality by avoiding any compression, then converted to a TIFF format with a 16-bit depth. Multiple objects, persons, animals and plants have been extracted from different scenes and pasted in some others, resulting in a set of twenty sliced pictures involving those different categories of sceneries. The splicing operations were done using *Adobe Photoshop CS6*.

The paper is organized as follows. In Section 2, we summarize the related work in the field of color constancy and image splicing detection with the illuminant color. Section 3 explains the physical principles used to estimate the illuminant color based on the dichromatic reflection model and the Lambertian model. In Section 4, we provide a step-by-step explanation of the method we are proposing to detect image forgery in addition to numerous experiments on spliced pictures to test their performances. The conclusion is given in the last section.

2 Related work

As mentioned previously, the illuminant color inconsistency is used to detect image splicing in many proposed methods. The earliest method applying the illuminant color analysis in image forensics has been proposed by Gholap and Bora[23]. The authors estimate the chromaticity of the illuminant color of different objects based on the dichromatic reflectance model and try to detect the changes in the model. Later on, Francis and Gholap[31] proposed a method to help dealing with the detection of the illuminant when encountering pictures that features human skin. However, this method turns out to be especially sensitive to the skin highlight regions. To avoid these constraints, Wu and Fang[25] estimate the illuminant color on each overlapping block under the Lambertian assumption, i.e., purely diffuse reflectance. For this, low-level statistics-based algorithms of illuminant estimation have been adapted for the specific image block. The angular error between the estimates of the blocks and those of some reference blocks is measured for the final decision of tampering. However, the method is practically limited by manual selection of reference blocks, thus the inappropriate reference blocks probably produce the inaccurate detection results.

Riess and Angelopouou[24] have proposed a physical-based method for local illuminant estimation, based on inverse-intensity chromaticity space. Both the illuminant and distance maps are used to identify image authenticity. Although this method can perform on rough highlight regions, manual interaction is needed to select the dominant illuminants. Furthermore, the authors do not provide any numerical criterion for splicing detection. Recently, De Carvalho and Riess[22] have developed a learning process of the illuminant colors for the detection of spliced images of people. The illuminant estimates for faces are performed using statistics-based[29] and physics-based[24] methods. These estimates are then used to automatically make tampering decision through a novel machine-learning approach. The proposed method requires only a small amount of human interactions and produces satisfactory results, but it has not shown any effectiveness on other types of images e.g., images containing plants, or animals.

In the field of color constancy, extensive methods have been presented[27]. Indeed, most illuminant color estimators typically assume globally uniform illumination. In other words, the spectral distribution of one light source is uniform across the scene and therefore the illuminant color is constant all over the image. However, in practice, many real-world images consist of more than one illuminant and thus often exhibit a mixture of different light sources. In order to use the illumination as an indicator of image splicing, we require multiple and local illuminant estimation. However, very few methods explicitly focus on this direction. In early research, color constancy for multiple illuminants has been proposed by Kuang and Xiong[33]. They used the modified local auto white-balance algorithm to solve the local illuminant for High-Dynamic-Range images. The illuminant estimation per pixel is performed through color information of its neighboring pixels, weighted by the spatial distance, luminance intensity difference and chromaticity. Later, Bleier and Riess have proposed a method[34] to determine multiple light sources using local illuminant estimation for super pixels which originates from the segmentation on the image. The common algorithms are applied to each super pixel independently. The final accurate illuminant per super pixel is determined using either the average of all combined estimates or machine learning regression. Gijsenij and Rui[35] have proposed a general color constancy method for multiple light sources. They apply the

existing color constancy algorithms to image patches in order to obtain local illuminant estimates. This method mainly focuses on scenes with two distinct light sources and their combination. The final estimation of two distinct illuminant colors is given either by clustering the illuminant estimates for patches or by incorporating spatial information with segmentation. Recently, Beigpour and Riess have developed a new method[36] to estimate the multiple illuminants and their spatial distribution, using an energy minimization strategy within a Conditional Random Field. They have also proposed two new datasets for multi-illuminant estimation. More recently, Joze and Drew have presented an exemplar-based color constancy method[37] for multiple illuminants. Mazin and Delon[32] have proposed a learning-free method based on the Planckian locus for the estimation of several illuminants which we adapted in our second method. The illuminant colors of the scene are obtained by projecting gray pixels on a Planckian locus in a specific chromaticity diagram. Van de Weijer and Gevers[29] have presented a framework, namely Grey-Edge, that systematically incorporates the well-known color constancy methods. Finally, given its omnipresence in an increasingly wide and varied range of application in the last years, it should be noted that Bianco and Cusano[38] developed a Convolutional Neural Network specifically designed to provide multiple local illuminant color estimations by working on image patches. Within a similar context, Shi and Loy[39] developed a Deep Specialized Network separated into two sub-networks: one makes multiple illuminant estimation hypotheses and the other selects one of them. In both of these papers, it is shown that the presented networks either achieve or outperform the state-of-the-art performance. We will now present the different physical models used to estimate illuminants in order to detect spliced regions.

3 Illuminant color estimation

Color constancy aims to estimate the chromaticity of the illuminant color and then to correct the image to a canonical light source using the diagonal model. The illumination estimation, which is thus the main part of color constancy, is applied in different fields such as image segmentation, image retrieval and object recognition. Furthermore, the illuminant color can also be an indicator of image tampering evidence because of the variation of light sources from two different scenes. The colors of an object observed in the image are determined by its actual color and the color of the light source. Therefore, the objects that are in the same scene but exposed to two different illuminants may appear of different colors.

In the method we are developing, the main task is indeed the estimation of these illuminant colors. We will show below that the different models stated from the formation of a color image can be of use when trying to estimate the illuminant color of a given region in a scene.

3.1 Color image formation

A color image taken by a linear device such as a digital camera is expressed as a vector of 3 pixel values (RGB), i.e. $p = (p_R, p_G, p_B)^T$. These values depend on the surface reflectance for body reflection component $S_b(\lambda, x)$, the spectral power distribution $E(\lambda)$ i.e. the color of the light source and the device sensitivity function $\rho(\lambda) = (\rho_R, \rho_G, \rho_B)^T$. Thus the image color at location x can be modeled as[40][41]:

$$p_c(x) = \int_\omega m_b(x)E(\lambda)S_b(\lambda, x)\rho_c(\lambda)d\lambda + \int_\omega m_S(x)E(\lambda)\rho_c(\lambda)d\lambda, \quad (1)$$

where c is a color pixel in (R, G, B), λ and ω being the interval of wavelength of the light and the visible spectrum, respectively. Moreover, as the first part of Equation 1 corresponds to the diffuse body or Lambertian reflectance and the second part corresponds to the interface or specular reflectance, $m_b(x)$ and $m_S(x)$ are the geometric scale factors for these respective types of reflectance, in that order. The surface reflectance $S_S(\lambda, x)$ of the interface component is assumed to be constant as the index of refraction does not significantly vary according to ω. Accordingly, $S_S(\lambda, x)$ does not appear in Equation 1 and is included in $m_S(x)$.

3.1.1 Dichromatic reflection model

The dichromatic reflection model[41] states that the light reflected from an inhomogeneous object is decomposed into two additive components: the diffuse or body reflection and the specular or interface reflection. The former corresponds to the Lambertian reflectance, while the latter is assumed to be similar to the spectral energy distribution of the incident light. The underlying assumption[40] for most dichromatic-based methods is that the pixels of an object surface fall on a plan in a RGB color space. Relying on at least two unparalleled plans that correspond to two different color surfaces, the color of the light source is estimated by finding an intersection of these planes. Some methods [23, 30, 42, 43] for illumination estimation propose to use the bright areas of the image such as highlights, specularities or white surfaces. Both these approaches assume that the color of the pixels in the highlighted regions is identical or similar to that of the light source. Although those dichromatic-based methods can perform well for the objects that show specular highlights, they require the highlight regions segmentation and suffer from the problem of similar object colors.

3.1.2 Lambertian model

Under the Lambertian assumption, the target image only has a diffuse reflection. It means that the Lambertian model ignores the specular reflection. As a result, Equation 1 used in the color image formation becomes:

$$p_c(x) = m(x) \int_\omega E(\lambda)S(\lambda, x)\rho_c(\lambda)d\lambda, \quad (2)$$

where $m(x)$ is the scale factor of the Lambertian surface and does not depend of the wavelength of the light. For

a given x, the reflected light color $p_c(x)$ can then be modeled as follows:

$$p_r c(x) = \begin{pmatrix} p_R \\ p_G \\ p_B \end{pmatrix} = \int_\omega E(\lambda) S(\lambda, x) \rho_c(\lambda) d\lambda. \quad (3)$$

Since $p_c(\lambda)$ is unknown and the spectral power distribution $E(\lambda)$ cannot be recovered from the discrete sensor measures, determining p_c is under constraints: it is therefore usual to estimate the illuminant color based on some strong assumptions. We will need two of these assumptions in the next part.

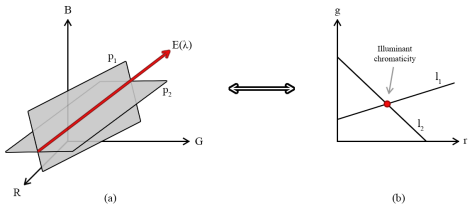

Figure 2: (a) Two dichromatic planes p_1 and p_2 in the RGB color space, (b) p_1 and p_2 mapped as two dichromatic lines l_1 and l_2 in the $r-g$ chromaticity space. l_1 and l_2 intersection is highlighted in red.

3.2 Illuminant color estimation

3.2.1 Illuminant color estimation using dichromatic lines

Gholap and Bora[23] have introduced a method to estimate the chromaticity of the illuminant color by using the specular regions of a pair of objects. The estimation is accomplished by finding an intersection point, i.e., the values of the illuminant chromaticity, of two dichromatic lines in the $r-g$ chromaticity space. First, two dichromatic planes corresponding to the two chosen specular regions must be found, as they represent the observations of our color signal by being the linear combination of the diffuse reflection vector and the specular reflection vector[40]. This is done by the application of principal component analysis, or PCA, on each of their pixels. It is used as a feature extraction method to get a better representation of the RGB values from our set of pixels, in the form of a two-dimensional space. After using an orthogonal transformation, the initial set of data is converted into a set of values of linearly uncorrelated variables which are the principal components of the PCA. We can obtain our two-dimensional feature space by projecting the data onto the plane defined by the first two principal components: they correspond to the eigenvectors with the two most significant eigenvalues, meaning that these components have the largest possible variance and that they are the most informative about our initial set of data. The two planes obtained from applying PCA on the sets of pixels from our regions are mapped in the $r-g$ chromaticity space using the following parameters:

$$r = \frac{R}{R+G+B}, \qquad g = \frac{G}{R+G+B}. \quad (4)$$

Any two specular regions of different colors can be used in illumination estimation.

This method suffers from several constraints: it needs an initial detection of specular highlights and the picture, including the sliced region, must contain specular highlights, these specularities should not be too small and the spliced regions and original areas ratio should stay balanced.

3.2.2 Illuminant color estimation using Planckian locus

Mazin and Delon[32] have proposed a learning-free method based on the Planckian locus to estimate the color of several illuminants. The method relies on two physical assumptions. The first one concerns the limit of feasible illuminants: the set of possible light sources is assumed to be modeled by using the Planckian locus of black-body radiators. The second physical assumption concerns the content of the image: it is assumed that there is at least an achromatic/gray surface that contains perfectly reflective pixels in the scene, which means that this achromatic surface is a region that depicts a color identical to the light source. From these assumptions, the illuminant can be calculated with the Planckian model, which states that the spectrum of light source $E(T,\lambda)$ emitted by a black body in thermal equilibrium at a definite temperature T is given by:

$$E(T,\lambda) = c_1 \lambda^{-5} \left[e^{\frac{c_2}{\lambda T}} - 1 \right]^{-1}, \quad (5)$$

where T is the temperature in Kelvin, λ corresponds to the wavelength and $c_1 = 3.74183 \times 10^{16}\ Wm^2$ and $c_2 = 1.4388 \times 10^{-2}\ mK$ are two constants. Although Equation 5 can be directly used to compute the spectrum of most light sources in the daily life, the results cannot be represented in chromaticity space. In our work, we use Mazin and Delon's[32] numerical approach based on the Planckian locus instead of directly using Equation 5. The Planckian locus is the path followed by the color of a black body in a given chromaticity space when the temperature of the black body changes. The black body is represented by the achromatic surface in the image. Note that not only most natural illuminants but also some typical artificial light sources can be estimated by the Planckian locus[44].

Figure 3a depicts the Planckian locus in the CIE (International Commission on Illumination) 1931 xy chromaticity diagram. The black line is a path that goes from deep red at low temperatures through orange, yellowish white, white and finally bluish white at high temperatures. The method we use is based on the following assumption: the various chromaticities of most illuminant colors are very close to the values found in the Planckian locus by studying achromatic pixels. The two chromaticity coordinates x and y are normalization of the tristimulus values XYZ and are obtained from pixels values in the RGB color space by the following transformation matrix given by CIE 1961 when the image origin is unknown: as follows:

$$\begin{bmatrix} X \\ Y \\ Z \end{bmatrix} = \frac{1}{0.17697} \begin{bmatrix} 0.49000 & 0.31000 & 0.20000 \\ 0.17697 & 0.81240 & 0.01063 \\ 0.00000 & 0.01000 & 0.99000 \end{bmatrix} \begin{bmatrix} R \\ G \\ B \end{bmatrix}, \quad (6)$$

$$x = \frac{X}{X+Y+Z}, \qquad y = \frac{Y}{X+Y+Z}, \quad (7)$$

with R, G and B the intensity of the red, blue and green channel values of a given pixel in the RGB color space, respectively.

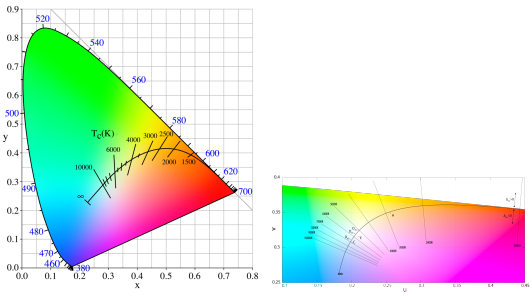

(a) CIE 1931 xy chromaticity diagram. (b) CIE 1960 uv chromaticity diagram.

Figure 3: Planckian locus in the CIE chromaticity diagram.

The Planckian locus can be computed using also the CIE 1960 color space, also known as MacAdam's uv chromaticity diagram[45], which is used in our algorithm. It is shown in Figure 3b. The uv diagram is represented by the two chromaticity coordinates u and v, obtained as follows:

$$u = \frac{4x}{12y - 2x + 3}, \qquad v = \frac{6y}{12y - 2x + 3}. \tag{8}$$

Figure 3b shows the Planckian locus depending on the different color temperatures in the CIE 1960 uv chromaticity diagram. For T, a color temperature in Kelvin located between 1000 K and 15000 K, the following values of u and v project the Planckian locus in the CIE 1960 uv chromaticity diagram:

$$u_P = \frac{0.860117757 + 1.54118254 \times 10^{-4} \times T + 1.28641212 \times 10^{-7} \times T^2}{1 + 8.42420235 \times 10^{-4} \times T + 7.08145163 \times 10^{-7} \times T^2}, \tag{9}$$

$$v_P = \frac{0.317398726 + 4.22806245 \times 10^{-5} \times T + 4.20481691 \times 10^{-8} \times T^2}{1 - 2.89741816 \times 10^{-5} \times T + 1.61456053 \times 10^{-7} \times T^2}. \tag{10}$$

Also, in order to provide a better sampling of these temperatures according to the human perception[46], we decide to use the Micro Reciprocal Degree (MIRED):

$$T_{MIRED} = \frac{10^6}{T}, \tag{11}$$

with T the color temperature in Kelvin and T_{MIRED} its MIRED value in reciprocal megaKelvin (MK^{-1}).

Different methods for the estimation of the illuminant have been proposed using the Planckian locus, with for example Lehman and Palm[43] and Finlayson and Schaefer[47] estimating the illumination chromaticity by intersecting the dichromatic line with the Planckian locus. In those cases, the illuminant color can be estimated even if there is only one surface in the scene. However, the image must be segmented into regions of homogeneous color, and these regions have to contain highlight pixels. Additionally, the methods work poorly for yellow and blue illuminated regions whose dichromatic lines have similar orientations to the Planckian locus. From this approach, Storring[48] proposes a method to estimate the illuminant color from observations of the skin color. It shows good performance on real-world images but requires prior knowledge about the camera parameters. The selection of achromatic pixels is done by projection on the Planckian locus and a voting procedure is used to obtain robust illuminant estimation.

The method of Mazin and Delon [32] has not a pre-segmentation processing. Moreover, it performs well for the scene of several illuminants. To estimate the illuminant color of a region, its achromatic pixels are first found by selecting the pixels of the region, projected in the uv chromaticity diagram, that are the closest to the Planckian locus. Then, an histogram of the MIRED temperatures estimated from the achromatic pixels of the region is built. These temperatures correspond to the dominant illuminants in the region: the histogram is considered to be a mixture of Gaussians, with each Gaussian distribution corresponding to one illuminant. We proceed with a small filtering to separate the major Gaussian distributions from the micro-peaks. Finally, an estimation of the illuminant is made by combining the Gaussian distributions that are left and projecting the corresponding temperature to the Planckian locus.

4 Detection of Image Splicing using Planckian Locus

4.1 Proposed method

We propose an adaptation of the method of Mazin and Delon [32] for image manipulation detection. The goal of this method is to compare estimations of the illuminant color related to different regions of the picture that will be retrieved via manual segmentation. The original paper assumed that a single illuminant is used in the whole scene: since the pictures we are working on are spliced, we chose to bring this method to the security field by making the illuminant estimation local. The way we estimate these illuminants is quicker and more reliable than the original method and we added a final representation of the picture showcasing the estimated illuminant colors to easily spot the possible anomalies in our pictures. Our algorithm is built as it follows:

1. All the pixels from each region of interest are plot in the CIE 1960 uv chromaticity diagram
2. The pixels close to the Planckian locus are labeled as achromatic and are projected on it
3. Their position on the Planckian locus corresponding to a particular temperature value, a weighted histogram is built
4. A Gaussian filter is applied on the histogram, which lets us retrieve the different Gaussian distributions that are represented
5. The most significant Gaussian distribution are kept and pixels from these Gaussians are used to estimate the illuminant color of the region
6. The illuminant color, originally estimated in the uv color space, is also converted to the RGB color space and gets more saturated for viewing purposes

7. The colors are applied on the regions of interest to easily spot the ones that differ

We will use the image (a) in Figure 4 where the object from the base presented on Figure 1 (b) has been pasted onto a new image. The chosen regions of interest in (b) correspond to the different objects in the scene we want to compare.

(a) (b)

Figure 4: (a) Spliced image, (b) Regions of interest.

As mentioned previously in Section 3.2.2, finding the achromatic pixels in an image plays an important role in determining the illuminant color of the scene. The achromatic pixels are the closest to the Planckian locus in uv chromaticity diagram and are assumed to have the same color as the light source. Hence, we start by finding the pixels in our image that are close to the Planckian locus when projected on the uv chromaticity diagram, with the use of Equations 6 to 10. To do so, we project each pixel of the image to the uv chromaticity diagram and find the point in the Planckian locus that satisfies the minimal Euclidean distance between it and the projected pixel:

$$p_{uv_{proj}} = \min_{\forall p_{PL} \in L} ||p_{uv} - p_P||^2, \tag{12}$$

with p_{uv} being a pixel of the image projected in the uv chromaticity diagram, L being the Planckian locus and $p_{uv_{proj}}$ the projection of p_{uv} on the Planckian locus. An example of a projection is shown in Figure 5. If the Euclidean distance between the pixel and its projection is less than a given threshold δ experimentally set at $\delta = 0.0125$, the pixel is potentially considered as an achromatic pixel, which means it needs to satisfy the following condition:

$$||p_{uv} - p_{uv_{proj}}||^2 < \delta. \tag{13}$$

This achromatic pixel lets us retrieve the temperature of its related black body radiator by looking at its position on the Planckian locus.

In Figure 6, the pixels from the different regions are projected on the uv chromaticity diagram. The ones satisfying Equation 13 are represented by red dots while those which don't are represented in black. For the sake of clarity, only 10% of the pixels appear in this graphic. We can already see that the achromatic pixels from region 3 are located in a lower area on the chromaticity diagram than the pixels from the other regions, which corresponds to a higher temperature in the Planckian locus.

Figure 7 highlights the pixels that have been selected. Note that if less than 5% of the pixels of a region are labeled as achromatic, no illuminant color will be estimated. Here, 99.5%, 97.4%, 74.2% and 99.7% of the pixels from respectively region 1, 2, 3 and 4 remain. A few pixels

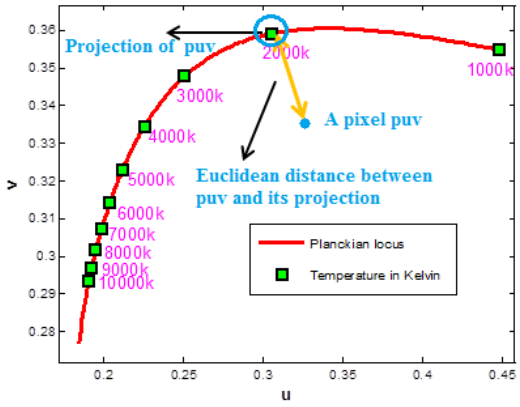

Figure 5: Projection of a pixel on the Planckian locus from the CIE 1960 uv chromaticity diagram.

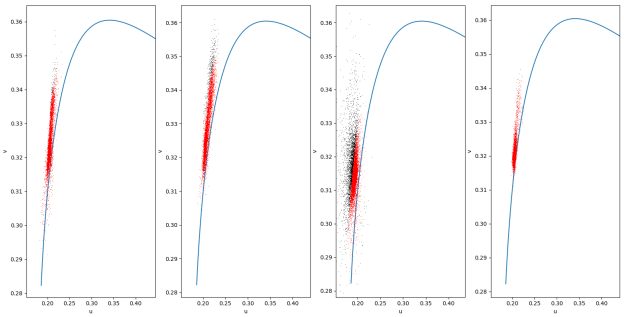

(a) (b) (c) (d)

Figure 6: Projection on the Planckian locus from the CIE 1960 uv chromaticity diagram of 10% of the pixels from (a) Region 1, (b) Region 2, (c) Region 3, (d) Region 4.

coming from the cup in region 3 have been labeled as chromatic and thus do not participate in the rest of the algorithm.

Figure 7: Achromatic pixels in the different regions.

In order to estimate the illuminant chromaticity of the region, we need to build the histogram of all the different temperatures detected from the achromatic pixels we gathered. As explained in Section 3.2.2 with Equation 11, this histogram is built in MIRED. To limit the influence of the darkest pixel, it is also weighted by the power of each pixel luminance value Y found in the CIE 1931 color space, as defined in Equation 6.

To estimate the illuminant, we have to extract the modes of histogram denoting the most frequent MIRED. These temperatures correspond to the dominant illuminants in the scene. Mazin and Delon[32] propose to use an *a contrario* detection method, but operating in this

way has a drawback: since it has to make the decision for each interval of histogram, it becomes really complex in the case of local regions of interest. In our method, we decide to first smooth the histogram with a Gaussian filter, which makes the histogram a mixture of Gaussians, each Gaussian distribution being considered as one illuminant.

To detect the different Gaussian distribution, we propose a new step in Mazin and Delon[32]'s method by using an *ad hoc* procedure. Firstly, we start by recording the color temperature which corresponds to a peak value in the histogram. This temperature value T_{mean} is considered as the mean of its corresponding Gaussian distribution. Secondly, the standard deviation σ is computed by analyzing the distribution values around T_{mean}. Having T_{mean} and σ at hand, we can now approximate a Gaussian distribution. To avoid parasites, we decided that if a given Gaussian distribution G_i is to be associated to an illuminant, it needs to satisfy the two rules stated below:

1. The ratio between the peak value of the Gaussian distribution P_i and the peak value of the whole histogram P_H must be equal or larger than a given threshold $\delta_1 = 0.05$: $\frac{P_i}{P_H} \geq \delta_1$

2. The normalized peak value of the Gaussian distribution, which is the ratio between the peak value of the Gaussian distribution P_i and the sum of each value h_j in the histogram, must be equal or larger than a given threshold $\delta_2 = 0.01$: $\frac{P_i}{\sum_{j=0}^{N_b} h_j} \geq \delta_2$ with N_b the total number of bins in the histogram

Figure 8 shows the histogram of our four regions. As said earlier, the achromatic pixels from region 3 seem to be of a higher temperature than the other regions. Note that the histogram is sorted in MIRED: the higher temperatures are on the left side while the lower ones are on the right. Note that we obtained the same results using Gaussian mixture models (GMMs) with the Expectation-Maximization (EM) algorithm but with a more important complexity.

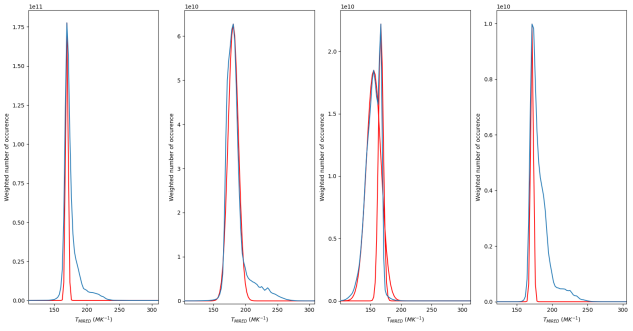

(a) (b) (c) (d)

Figure 8: Histogram of the achromatic pixels in from (a) Region 1, (b) Region 2, (c) Region 3, (d) Region 4 (original histograms in blue, estimations in red).

Now that the distribution has been validated, we select all the achromatic pixels in the $[T_{mean}-\sigma, T_{mean}+\sigma]$ range and approximate their value to estimate the corresponding illuminant. If multiple Gaussian distributions in the region have been detected, the procedure explained above is repeated but a weighted mean is operated to estimate the final illuminant, using the peak values of the Gaussian distributions as weights for the achromatic pixels.

In Figure 9, we can see that regions 1 and 4 illuminants estimations are pretty close to each others but regions 2 and 3 seem more distant. While the object from region 3 does indeed come from an other picture, the object from region 2 comes from the original image: a suitable explanation would be that the object from region 2 is really close to the light source located on the right, whereas the objects from region 1 and 4 are more close to the light source located on the left.

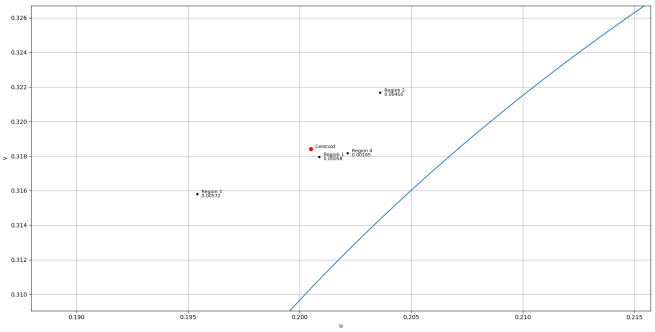

Figure 9: Estimation of the illuminant color in the CIE 1960 uv chromaticity diagram.

Moreover, Figure 9 only gives us information coming from the uv color space. Another point of view could be acquired by converting those colors back to the RGB color space. Since the luminance value, represented by Y, is needed when going from the xyz to the XYZ color space, a new value of $Y = 0.8$ has been arbitrarily given. Finally, since our the pixels used to estimate our illuminant colors are achromatic, the color seen in the RGB color space will, by definition, have a low saturation. As a consequence, we artificially enhance its color saturation value in the HSV color space before visualizing it, for comparison purposes only:

$$S_E = S + 0.2 * (255 - S) \tag{14}$$

with S_E being the enhanced saturation value and S being the normalized original one. In Figure 10, region 3 definitely stands out by having a greenish color as opposed to the other three regions having an orange color.

(a) (b)

Figure 10: (a) Spliced image, (b) Estimation of the illuminant color in the RGB color space, with enhanced saturation.

4.2 Results

To validate our method for image splicing detection, we perform experiments on multiple images that have been taken and manipulated for the purposes of this paper, as explained in Section 1. Some results of detection are showcased below in the following sections and a last section describes and explains the problems that were met during the experiments.

4.2.1 Experiment 1

There is no interaction between each region of interest we can select in an image. The color estimation we get at the end of the algorithm depends only of the selected pixels. Therefore, since the final decision is made by comparing the different colors given by the algorithm, an experiment dedicated to a non-spliced image is unnecessary, as it is equivalent to only analyze the non-spliced regions of a spliced image.

In the first experiment, we will analyze a spliced image taken outdoors and containing an object coming from an image taken indoors. In Figure 11, the camera corresponding to region 4 is the object cropped from an other image. We can also note that region 6 is a gray-colored reflective surface and a red traffic light directly casts a red light on it.

(a) (b)

Figure 11: (a) Spliced image, (b) Regions of interest.

In Figure 12, we can see that the red parts of region 6 have been discarded as they are not close to the Planckian locus when projected on the uv chromaticity diagram. Only the white-gray text remains.

Figure 12: Achromatic pixels in the different regions.

In Figure 13, we can observe that the illuminant color linked to the spliced region 4 is far away from the rest of the regions.

Finally, Figure 14 gives us an estimation of the illuminant color of each object. Region 4 illuminant color is yellow, regions 1, 2, 3, 5, 7 colors are blueish, while region 6 color is more purple: it may come from the fact that

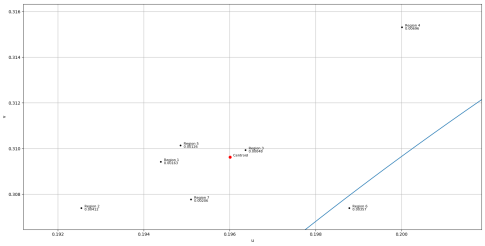

Figure 13: Estimation of the illuminant color in the CIE 1960 uv chromaticity diagram.

two light sources are casted on region 6, both the bluish day light found in the other regions minus region 4 and the red traffic light. The algorithm succeeded in showing us that region 4 was spliced.

(a) (b)

Figure 14: (a) Spliced image, (b) Estimation of the illuminant color in the RGB color space, with enhanced saturation.

4.2.2 Experiment 2

We apply our algorithm to the spliced picture we studied in the previous method. This time, we are using new regions of interest, seen in Figure 15 (b).

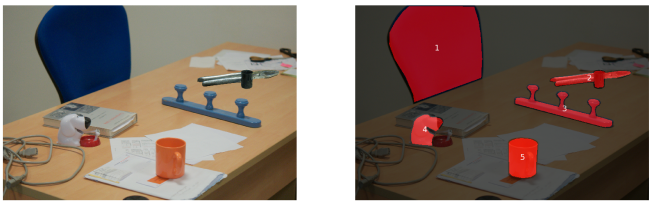

(a) (b)

Figure 15: (a) Spliced image, (b) Regions of interest.

As we can see in F igure 16 (a), only 0.4% of the pixels from region 1 are close enough to the Planckian locus to be considered as achromatic, the other 99.6% being represented in black. This region will therefore not be used in the next steps of the algorithm.

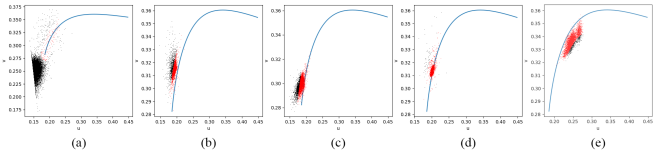

(a) (b) (c) (d) (e)

Figure 16: Projection on the Planckian locus from the CIE 1960 uv chromaticity diagram of 10% of the pixels from (a) Region 1, (b) Region 2, (c) Region 3, (d) Region 4, (e) Region 5.

The results obtained in Figure 17 and 18 are not satisfying: every remaining object has a different estimated illuminant color. This is explained by the fact that region 2 and 3 depict objects that are coated in an intense color and their achromatic pixels contain more information about their color than the light source they reflect. The regions 1 and 4 which are gray and white are the only ones that can give us an acceptable illuminant color estimation.

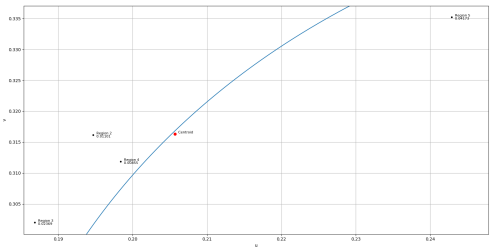

Figure 17: Estimation of the illuminant color in the CIE 1960 *uv* chromaticity diagram.

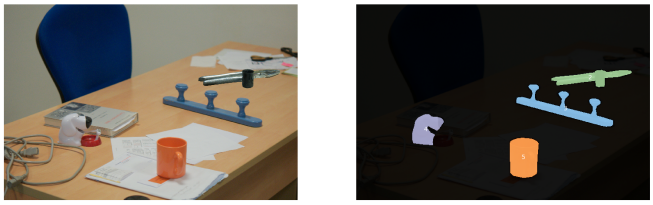

(a) (b)

Figure 18: (a) Spliced image, (b) Estimation of the illuminant color in the *RGB* color space, with enhanced saturation.

4.2.3 Experiment 3

In our third experiment, we will examine a picture featuring people. The original picture has been taken indoors in a closed environment and contains one person. The same person has been photographed outdoors, thus taken with a different light source, then cropped and pasted in the first picture, resulting in Figure 19 (a).

(a) (b)

Figure 19: (a) Spliced image, (b) Regions of interest

It is difficult to analyze Figure 20 properly as regions belonging to the spliced person are located next to regions belonging to the original picture. However, let us take into account that these regions go by pairs or triplets considering their nature: regions 1 and 4 depict the person's face, regions 3 and 7 depict his hand, regions 2 and 5 depict his shirt and region 6 and 8/9 depict his trousers, the first region cited being part of the original picture and the second/third being from the spliced region. We can see that the spliced regions are always under the Planckian locus while the original are always above - or slightly below in the case of region 1. The global illuminant color palette has shifted downward when comparing the spliced regions to the original ones. The spreading of the illumination color estimation belonging to the same picture come from the fact that we try to compare areas of different nature, with some of them, like the skin, having a natural color.

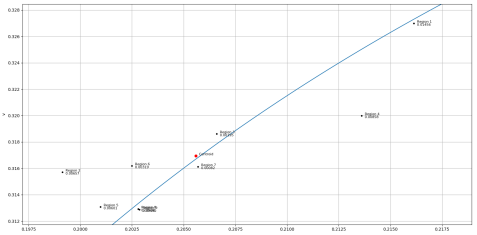

Figure 20: Estimation of the illuminant color in the CIE 1960 *uv* chromaticity diagram

In Figure 21, we can indeed see that the regions related to the spliced person have been exposed to a more red light source than the original picture, taken indoors.

(a) (b)

Figure 21: (a) Spliced image, (b) Estimation of the illuminant color in the *RGB* color space, with enhanced saturation

4.2.4 Discussion

Finally, the consequences of the multiple light sources are visible with our approach. As we have seen in Figure 14, when analyzing the final picture given by the algorithm, it is important to take into account the fact that some objects might receive multiple light sources and therefore get an illuminant color rather different from the other objects, even if it has not been spliced.

To estimate the illuminant color, the algorithm tries to find the achromatic pixel contained in the regions based on the second physical assumption we made in Section 3.2.2: there is at least an achromatic surface that

contains perfectly reflective pixels in the scene, this surface depicting a color identical to the light source. It first means that the algorithm will not give acceptable results if the studied surfaces do not contain a sufficiently high amount of achromatic pixels. However, an achromatic surface do not necessarily mean that it is the sign of a near-black-body radiator either. It may simply be the natural color of the object. Even if most of the chromatic pixels are discarded when projected on the Planckian locus, the remaining pixels may not be related to a reflective surface. The consequence is that to get significant results, it is preferable to select regions of interest that correspond to naturally white or gray colored objects. Otherwise, if an picked area is of a high-saturated color, it should be compared to areas of similar design, like a wall with an other wall or a shirt with an other shirt. It is also the reason why when pictures involve people, the algorithm works best if these people possess a similar skin-tone.

5 Conclusion

In this paper, we introduce a method to detect image splicing operations, a popular image forgery technique consisting in cropping a region from a given image and pasting it onto an other. We have proposed the adaptation of a method based on the Lambertian model, adding a way to locally estimate the illuminant color and easily compare multiple regions of an image.

This learning-free approach gives us good results and is easy to apply, as it does not need a precise segmentation of the regions of interest. However, these regions need not to be bright-colored as it interferes with the illuminant color estimation. Otherwise, colored objects of similar nature can be used for comparison.

When coming across a suspicious image, our method involves an analysis of the inconstancies in an estimation of the scene illuminant color, it also returns a colored image acting as a decision support and either representing a "tamper score" in the form of a heat map or a direct estimation of the illuminant color.

References

[1] E. Facebook and Qualcomm, "A focus on efficiency," (2013).

[2] F. Richter, "Smartphones cause photography boom," (2017).

[3] A. Hadland, D. Cambell, and P. Lambert, "The state of news photography: the lives and livelihoods of photojournalists in the digital age," Reuters Institute for the Study of Journalism (2015).

[4] H. Farid, "Digital doctoring: Can we trust photographs?" (2009).

[5] Z. B. Parry, "Digital manipulation and photographic evidence: defrauding the courts one thousand words at a time," U. Ill. JL Tech. & Pol'y p. 175 (2009).

[6] H. Farid, "Image forgery detection," IEEE Signal processing magazine **26**, 16–25 (2009).

[7] H. T. Sencar and N. Memon, "Overview of state-of-the-art in digital image forensics," in "Algorithms, Architectures and Information Systems Security," (World Scientific, 2009), pp. 325–347.

[8] H. Pearson, "Image manipulation: Csi: cell biology," (2005).

[9] I. Cox, M. Miller, J. Bloom, J. Fridrich, and T. Kalker, *Digital watermarking and steganography* (Morgan Kaufmann, 2007).

[10] B. Mahdian and S. Saic, "A bibliography on blind methods for identifying image forgery," Signal Processing: Image Communication **25**, 389–399 (2010).

[11] X. Lin, J.-H. Li, S.-L. Wang, F. Cheng, X.-S. Huang *et al.*, "Recent advances in passive digital image security forensics: A brief review," Engineering **4**, 29–39 (2018).

[12] A. C. Popescu and H. Farid, "Statistical tools for digital forensics," in "International Workshop on Information Hiding," (Springer, 2004), pp. 128–147.

[13] Y. Q. Shi, C. Chen, and W. Chen, "A natural image model approach to splicing detection," in "Proceedings of the 9th workshop on Multimedia & security," (ACM, 2007), pp. 51–62.

[14] W. Chen, Y. Q. Shi, and W. Su, "Image splicing detection using 2-d phase congruency and statistical moments of characteristic function," in "Security, Steganography, and Watermarking of Multimedia Contents IX," , vol. 6505 (International Society for Optics and Photonics, 2007), vol. 6505, p. 65050R.

[15] B. Bayar and M. C. Stamm, "A deep learning approach to universal image manipulation detection using a new convolutional layer," in "Proceedings of the 4th ACM Workshop on Information Hiding and Multimedia Security," (ACM, 2016), pp. 5–10.

[16] Y. Rao and J. Ni, "A deep learning approach to detection of splicing and copy-move forgeries in images," in "2016 IEEE International Workshop on Information Forensics and Security (WIFS)," (IEEE, 2016), pp. 1–6.

[17] J. Lukas, J. Fridrich, and M. Goljan, "Digital camera identification from sensor pattern noise," IEEE Transactions on Information Forensics and Security **1**, 205–214 (2006).

[18] M. K. Johnson and H. Farid, "Exposing digital forgeries through chromatic aberration," in "Proceedings of the 8th workshop on Multimedia and security," (ACM, 2006), pp. 48–55.

[19] M. K. Johnson and H. Farid, "Exposing digital forgeries by detecting inconsistencies in lighting," in "Proceedings of the 7th workshop on Multimedia and security," (ACM, 2005), pp. 1–10.

[20] E. Kee and H. Farid, "Exposing digital forgeries from 3-d lighting environments," in "Information Forensics and Security (WIFS), 2010 IEEE International Workshop on," (IEEE, 2010), pp. 1–6.

[21] J. F. O'Brien and H. Farid, "Exposing photo manipulation with inconsistent reflections." ACM Trans. Graph. **31**, 4–1 (2012).

[22] T. J. De Carvalho, C. Riess, E. Angelopoulou, H. Pedrini, and A. de Rezende Rocha, "Exposing digital image forgeries by illumination color classification," IEEE Transactions on Information Forensics and Security **8**, 1182–1194 (2013).

[23] S. Gholap and P. Bora, "Illuminant colour based image forensics," in "TENCON 2008-2008 IEEE Region 10 Conference," (IEEE, 2008), pp. 1–5.

[24] C. Riess and E. Angelopoulou, "Scene illumination as an indicator of image manipulation," in "International Workshop on Information Hiding," (Springer, 2010), pp. 66–80.

[25] X. Wu and Z. Fang, "Image splicing detection using illuminant color inconsistency," in "Multimedia Information Networking and Security (MINES), 2011 Third International Conference on," (IEEE, 2011), pp. 600–603.

[26] D. Cozzolino, D. Gragnaniello, and L. Verdoliva, "Image forgery localization through the fusion of camera-based, feature-based and pixel-based techniques," in "2014 IEEE International Conference on Image Processing (ICIP)," (IEEE, 2014), pp. 5302–5306.

[27] A. Gijsenij, T. Gevers, and J. Van De Weijer, "Computational color constancy: Survey and experiments," IEEE Transactions on Image Processing **20**, 2475–2489 (2011).

[28] D. S. Vidyadharan and S. M. Thampi, "Illuminant color inconsistency as a powerful clue for detecting digital image forgery: A survey," in "The International Symposium on Intelligent Systems Technologies and Applications," (Springer, 2017), pp. 279–297.

[29] J. Van De Weijer, T. Gevers, and A. Gijsenij, "Edge-based color constancy," IEEE Transactions on image processing **16**, 2207–2214 (2007).

[30] R. T. Tan, K. Ikeuchi, and K. Nishino, "Color constancy through inverse-intensity chromaticity space," in "Digitally Archiving Cultural Objects," (Springer, 2008), pp. 323–351.

[31] K. Francis, S. Gholap, and P. Bora, "Illuminant colour based image forensics using mismatch in human skin highlights," in "Communications (NCC), 2014 Twentieth National Conference on," (IEEE, 2014), pp. 1–6.

[32] B. Mazin, J. Delon, and Y. Gousseau, "Estimation of illuminants from projections on the planckian locus," IEEE Transactions on Image Processing **24**, 1944–1955 (2015).

[33] J. Kuang and W. Xiong, "Color constancy for multi-illuminants high-dynamic-range scenes," in "Color and Imaging Conference," (Society for Imaging Science and Technology, 2008), pp. 56–60.

[34] M. Bleier, C. Riess, S. Beigpour, E. Eibenberger, E. Angelopoulou, T. Tröger, and A. Kaup, "Color constancy and non-uniform illumination: Can existing algorithms work?" in "Computer Vision Workshops (ICCV Workshops), 2011 IEEE International Conference on," (IEEE, 2011), pp. 774–781.

[35] A. Gijsenij, R. Lu, and T. Gevers, "Color constancy for multiple light sources," IEEE Transactions on Image Processing **21**, 697–707 (2012).

[36] S. Beigpour, C. Riess, J. Van De Weijer, and E. Angelopoulou, "Multi-illuminant estimation with conditional random fields," IEEE Transactions on Image Processing **23**, 83–96 (2014).

[37] H. R. V. Joze and M. S. Drew, "Exemplar-based color constancy and multiple illumination," IEEE transactions on pattern analysis and machine intelligence **36**, 860–873 (2014).

[38] S. Bianco, C. Cusano, and R. Schettini, "Single and multiple illuminant estimation using convolutional neural networks," IEEE Transactions on Image Processing **26**, 4347–4362 (2017).

[39] W. Shi, C. C. Loy, and X. Tang, "Deep specialized network for illuminant estimation," in "European Conference on Computer Vision," (Springer, 2016), pp. 371–387.

[40] S. Tominaga and B. A. Wandell, "Standard surface-reflectance model and illuminant estimation," JOSA A **6**, 576–584 (1989).

[41] S. A. Shafer, "Using color to separate reflection components," Color Research & Application **10**, 210–218 (1985).

[42] G. D. Finlayson and G. Schaefer, "Solving for colour constancy using a constrained dichromatic reflection model," International Journal of Computer Vision **42**, 127–144 (2001).

[43] T. M. Lehmann and C. Palm, "Color line search for illuminant estimation in real-world scenes," JOSA A **18**, 2679–2691 (2001).

[44] D. B. Judd, D. L. MacAdam, G. Wyszecki, H. Budde, H. Condit, S. Henderson, and J. Simonds, "Spectral distribution of typical daylight as a function of correlated color temperature," Josa **54**, 1031–1040 (1964).

[45] K. L. Kelly, "Lines of constant correlated color temperature based on macadamâĂŹs (u, v) uniform chromaticity transformation of the cie diagram," JOSA **53**, 999–1002 (1963).

[46] I. G. Priest, "A proposed scale for use in specifying the chromaticity of incandescent illuminants and various phases of daylight," JOSA **23**, 41–45 (1933).

[47] G. Finlayson and G. Schaefer, "Single surface colour constancy," in "Color and Imaging Conference," (Society for Imaging Science and Technology, 1999), pp. 106–113.

[48] M. Storring, H. J. Andersen, and E. Granum, "Estimation of the illuminant colour from human skin colour," in "Automatic Face and Gesture Recognition, 2000. Proceedings. Fourth IEEE International Conference on," (IEEE, 2000), pp. 64–69.